Monthly Notices
of the
ROYAL ASTRONOMICAL SOCIETY

MNRAS **444,** 700–710 (2014) doi:10.1093/mnras/stu1411

Radio galaxies and their magnetic fields out to $z \leq 3$

J. K. Banfield,[1,2★] D. H. F. M. Schnitzeler,[3] S. J. George,[4] R. P. Norris,[1] T. H. Jarrett,[5] A. R. Taylor[5,6] and J. M. Stil[7]

[1]*CSIRO Australia Telescope National Facility, PO Box 76, Epping, NSW 1710, Australia*
[2]*Research School of Astronomy and Astrophysics, Australian National University, Weston Creek, ACT 2611, Australia*
[3]*Max Planck Institut fur Radioastronomie, D-53121 Bonn, Germany*
[4]*Astrophysics and Space Research Group, School of Physics and Astronomy, University of Birmingham, Birmingham B15 2TT, UK*
[5]*Astronomy Department, University of Cape Town, Rondebosch 7701, Republic of South Africa*
[6]*Department of Physics, University of the Western Cape, Bellville 7535, Republic of South Africa*
[7]*Department of Physics and Astronomy, The University of Calgary, 2500 University Drive NW, Calgary, AB T2N 1N4, Canada*

Accepted 2014 July 11. Received 2014 July 8; in original form 2013 November 14

ABSTRACT

We present polarization properties at 1.4 GHz of two separate extragalactic source populations: passive quiescent galaxies and luminous quasar-like galaxies. We use data from the *Wide-Field Infrared Survey Explorer* to determine the host galaxy population of the polarized extragalactic radio sources. The quiescent galaxies have higher percentage polarization, smaller radio linear size, and 1.4 GHz luminosity of $6 \times 10^{21} < L_{1.4} < 7 \times 10^{25}$ W Hz^{-1}, while the quasar-like galaxies have smaller percentage polarization, larger radio linear size at radio wavelengths, and a 1.4 GHz luminosity of $9 \times 10^{23} < L_{1.4} < 7 \times 10^{28}$ W Hz^{-1}, suggesting that the environment of the quasar-like galaxies is responsible for the lower percentage polarization. Our results confirm previous studies that found an inverse correlation between percentage polarization and total flux density at 1.4 GHz. We suggest that the population change between the polarized extragalactic radio sources is the origin of this inverse correlation and suggest a cosmic evolution of the space density of quiescent galaxies. Finally, we find that the extragalactic contributions to the rotation measures (RMs) of the nearby passive galaxies and the distant quasar-like galaxies are different. After accounting for the RM contributions by cosmological large-scale structure and intervening Mg II absorbers we show that the distribution of intrinsic RMs of the distant quasar-like sources is at most four times as wide as the RM distribution of the nearby quiescent galaxies, if the distribution of intrinsic RMs of the *WISE*–Star sources itself is at least several rad m^{-2} wide.

Key words: galaxies: active – galaxies: evolution – galaxies: magnetic fields – radio continuum: galaxies.

1 INTRODUCTION

Tucci & Toffolatti (2012) recently found that the intrinsic percentage polarization of extragalactic radio sources (ERS) at frequencies $\geq$20 GHz is between 2 and 5 per cent, independent of flux density. These results were confirmed by Massardi et al. (2013) using the Australia Telescope 20 GHz (AT20G) Survey, while Sadler et al. (2006) suggest that there is a trend that fainter sources tend to have higher percentage polarization. This anticorrelation between percentage polarization and total flux density has also been suggested at 1.4 GHz by Mesa et al. (2002), Tucci et al. (2004), Taylor et al. (2007), Subrahmanyan et al. (2010), and Grant et al. (2010). Recently, Hales (2013) found no evidence for this trend and attribute the previous results to selection effects consistent with the reasoning by Massardi et al. (2013). As a result the anticorrelation of percentage polarization with total flux density, if it exists, remains a mystery.

The first studies of increasing percentage polarization with decreasing flux density came from Mesa et al. (2002) and Tucci et al. (2004), and both suggested that a population change of ERS at fainter flux densities was the cause. Taylor et al. (2007) went on to suggest that the cause was a result of a change in the fraction of radio quiet active galactic nuclei (AGN). Most recently, Rudnick & Owen (2014) examined the polarization properties of radio sources down to $S_{1.4\,\mathrm{GHz}} > 15$ μJy in The Great Observatories Origins Deep Field Survey North field (GOODS-N; Morrison et al. 2010) and suggest a population change around a polarized flux density of 1 mJy. Studies into the intrinsic properties of polarized ERS by Banfield et al. (2011) show a trend of increasing percentage polarization with

★E-mail: Julie.Banfield@csiro.au

decreasing luminosity and no trend with redshift, later confirmed by Hammond, Robishaw & Gaensler (2012). Subrahmanyan et al. (2010) suggest that this anticorrelation between percentage polarization and total flux density is likely to be a transition from Fanaroff & Riley (1974) type II (FRII)-dominated to FRI-dominated populations, while the results by Grant et al. (2010) imply that the higher percentage polarization may be originating in the lobe-dominated structure and not in beamed BL Lac objects. However, Shi et al. (2010) found no dependence on ERS environment when comparing highly polarized (>30 per cent) ERS with their low polarized counterparts. Shi et al. (2010) went on to suggest that intrinsic properties of magnetic field ordering, thermal plasma density, and magnetic field orientation to the line of sight are the root cause for highly polarized ERS.

In this paper, we present an analysis of 1.4 GHz polarized ERS in combination with optical spectroscopic data in order to explore this anticorrelation between percentage polarization and flux density. We probe polarized radio emission out to high redshifts and examine the magnetic fields within different ERS populations. We outline the sample selection in Section 3 and the nature of the polarized sources is discussed in Section 4. Section 5 describes the selection effects of our data, we discuss our findings in Section 6, and conclusions are presented in Section 7.

The cosmological parameters used throughout this paper are $\Omega_\lambda = 0.7$, $\Omega_M = 0.3$, and $H_0 = 70$ km s^{-1} Mpc^{-1}. We define the spectral index α as $S \propto \nu^\alpha$.

2 OBSERVATIONAL INDICATIONS OF COSMIC MAGNETIC FIELDS

2.1 Measuring polarization

All ERS emit radiation that is partially polarized and a measurement of all four Stokes parameters provides the necessary information to completely describe the polarization state of the electromagnetic radiation received from a radio source. Stokes I represents the total amount of radiation received, Stokes Q and Stokes U contain the linearly polarized information, while Stokes V contains the circularly polarized information. The linearly polarized flux density of a radio source is calculated by

$$P = \sqrt{Q^2 + U^2}, \tag{1}$$

and the percentage polarization is calculated by

$$\Pi = \left(\frac{\text{total polarized flux}}{\text{total flux}}\right) \times 100\,\text{per cent} = \frac{P}{S} \times 100\,\text{per cent}. \tag{2}$$

The statistical distribution of the noise when measuring polarized intensity is non-Gaussian and has a non-zero mean. Therefore, the resulting value of P can be biased high depending on the signal-to-noise ratio. The removal of this bias can be estimated as $P_0 = \sqrt{P^2 - \sigma^2}$ for a signal-to-noise ratio greater than 4 (Simmons & Stewart 1985). Also, errors derived from the least-squares approach will be too small (Wardle & Kronberg 1974).

2.2 Faraday rotation

The amount of Faraday rotation of polarized radio waves provides information on the strength and structure of the magnetic field along the line of sight, and depends on three factors: (1) the wavelength of the emission; (2) the electron density of the medium; and (3) the strength of the line-of-sight component of the magnetic field in the medium. Expressed in equation form

$$\Phi = \lambda^2 \left(0.812 \int n_e \boldsymbol{B} \cdot \mathrm{d}\boldsymbol{l}\right)\ \text{rad}, \tag{3}$$

where $\boldsymbol{B}$ is the magnetic field (μG), d$\boldsymbol{l}$ is an infinitesimal distance along the line of sight towards the observer (pc), λ is the observing wavelength (m), and n_e is the electron density (cm^{-3}). The rotation measure (RM) is given by

$$\mathrm{RM} = 0.812 \int n_e \boldsymbol{B} \cdot \mathrm{d}\boldsymbol{l}\ \ \text{rad m}^{-2}, \tag{4}$$

and is integrated from the source of the polarized radio waves to the observer. A positive RM indicates that the magnetic field component along the line-of-sight points towards the observer, while a magnetic field pointing away from the observer produces a negative RM.

Many factors contribute to the observed RMs of ERS, such as the Earth's ionosphere ($\mathrm{RM_{ion}}$), the Milky Way foreground ($\mathrm{RM_{MW}}$), and any Faraday screens that could be intrinsic to the sources or lie between the source of the emission and the Milky Way, which we shall we refer to as the 'extragalactic RM' ($\mathrm{RM_{ERS}}$). The sum of all these contributions is the RM that is measured as

$$\mathrm{RM} = \mathrm{RM_{ion}} + \mathrm{RM_{MW}} + \mathrm{RM_{ERS}}, \tag{5}$$

where $\mathrm{RM_{ion}}$ is typically 1 to 2 rad m^{-2} (Sotomayor-Beltran et al. 2013). In Section 4.4, we derive a new method for extracting the $\mathrm{RM_{ERS}}$ for different radio source populations.

3 SAMPLE SELECTION

3.1 Rotation measure and redshift catalogue

We used data from the Hammond et al. (2012) catalogue, which contain spectroscopic redshifts for 4003 polarized radio sources from the RM catalogue of Taylor, Stil & Sunstrum (2009) at 1.4 GHz with a declination $\delta \geq -40^\circ$ and a flux density $S_{1.4\,\mathrm{GHz}} \geq 11$ mJy in the redshift range $0 < z < 5.3$. The polarization information comes from the National Radio Astronomy Observatory Very Large Array Sky Survey (NVSS; Condon et al. 1998) which has an angular resolution of 45 arcsec and includes only those sources with a signal-to-noise ratio greater than 8 so that the noise bias correction for polarized flux density is negligible (Simmons & Stewart 1985; George, Stil & Keller 2012). Hammond et al. (2012) extracted redshifts from optical counterparts in the NASA/IPAC Extragalactic Database (NED; Helou et al. 1991), Set of Identifications, Measurements and Bibliography for Astronomical Data (SIMBAD; Wenger et al. 2000), Sloan Digital Sky Survey (SDSS; York et al. 2000), Six-degree Field Galaxy Survey (6dFGS; Jones et al. 2009), Two-degree Field Galaxy Redshift Survey (2dFGRS; Colless et al. 2001), and the 2dF QSO Redshift survey/6dF QSO Redshift survey (2QZ/6QZ; Croom et al. 2004).

3.2 Wide-field infrared survey explorer

The *Wide-field Infrared Survey Explorer* (*WISE*; Wright et al. 2010) surveyed the sky at wavelengths 3.4, 4.6, 12, and 22 μm with a 5σ point source sensitivity in unconfused regions of at least 0.08, 0.11, 1.0, and 6.0 mJy and angular resolutions of 6.1, 6.4, 6.5, and 12.0 arcsec. This sensitivity depends on the ecliptic latitude, with the poles having the greatest depth (Jarrett et al. 2011). The selection of these four bands makes *WISE* an excellent instrument for studies of stellar structure and interstellar processes of galaxies.

Table 1. Distribution of polarized NVSS sources from the Hammond et al. (2012) catalogue with a 5σ detection in each *WISE* band.

WISE band	*N*	Fraction of sources detected
3.4 μm	3741	93.5 ± 1.5 per cent
4.6 μm	3693	92.3 ± 1.5 per cent
12 μm	2729	68.2 ± 1.3 per cent
22 μm	1440	40.0 ± 1.1 per cent
Any Band	3747	93.6 ± 1.5 per cent

The two shorter bands trace the stellar mass distribution in galaxies and the longer wavelengths map the warm dust emission and polycyclic aromatic hydrocarbon emission, both tracing the current star formation activity.

Using the optical counterparts from the Hammond et al. (2012) catalogue, we matched 3747 polarized radio sources to within 5 arcsec of their *WISE* ALL Sky Source Catalogue[1] (Wright et al. 2010) counterparts down to a 5σ detection in at least one of the four *WISE* bands. Table 1 lists the distribution of sources in the four *WISE* bands.

4 NATURE OF POLARIZED RADIO SOURCES

The key findings of this section are summarized in Table 2.

4.1 *WISE* colours of polarized ERS

The *WISE* [4.6] − [12] and [3.4] − [4.6] colour–colour diagram is a good tool to distinguish different galaxy populations as outlined by the coloured shapes in Fig. 1, which have been defined by Wright et al. (2010) and Jarrett et al. (2011). Infrared emission dominated by light from evolved stars is found near zero colour, stretching to redder colours along the [4.6] − [12] axis towards more luminous evolved populations as traced by the 12 μm light and the power-law mid-infrared spectrum of AGN dominates the redder *WISE* colours in [3.4] − [4.6] (Jarrett et al. 2011; Stern et al. 2012). The general 'AGN' region covering quasi-stellar objects (QSOs) to Seyfert galaxies, as defined by Jarrett et al. (2011), is illustrated by the box shown in upper right of Fig. 1 (hereafter *WISE*–AGN). The region redward of the AGN box is populated by the most luminous infrared galaxies, while the region defined to be dominated by the infrared emission from starlight is defined by the box shown in the lower left of Fig. 1 (hereafter *WISE*–Star). The dots in Fig. 1 show the 2724 polarized NVSS ERS with a 5σ *WISE* detection in the 3.4, 4.6, and 12 μm bands. The polarized ERS in our sample clearly fall primarily in these two regions, with 266 polarized ERS in the region defined as *WISE*–Star and 2056 ERS in the *WISE*–AGN region.

In Fig. 2, we plot the percentage polarization of the sources from Fig. 1 as a function of the *WISE* colours. Fig. 2(a) shows the [4.6] − [12] *WISE* colour and Fig. 2(b) shows the [3.4] − [4.6] *WISE* colour along with the boundary of the *WISE*–AGN (black lines) and *WISE*–Star (red dashed lines) regions. The mean percentage polarization of the *WISE*–AGN ERS $\langle\Pi_{\rm AGN}\rangle = 3.6 \pm 0.2$ per cent (median $\Pi_{\rm AGN} = 3.2$ per cent) and for the *WISE*–Star ERS $\langle\Pi_{\rm Star}\rangle = 10.0 \pm 0.5$ per cent (median $\Pi_{\rm Star} = 7.5$ per cent). The polarized ERS that fall into the *WISE*–Star region show a higher percentage polarization by a factor of 3 than the polarized ERS in the *WISE*–AGN region.

The distribution of total flux density ($S_{1.4\,\rm GHz}$) and polarized flux density ($P_{1.4\,\rm GHz}$) can be seen in Fig. 3(a). The polarized *WISE*–AGN ERS are indicated by black dots, while the polarized *WISE*–Star ERS are indicated by red dots; the solid diagonal lines indicate $\Pi = 1$, 10, and 100 per cent. We split the sample into two flux density bins (1) $S_{1.4\,\rm GHz} > 100$ mJy and (2) $S_{1.4\,\rm GHz} \leq 100$ mJy which results in a similar number of sources with $S_{1.4\,\rm GHz} \leq 100$ mJy for both polarized ERS populations. We plot the percentage polarization distribution of the two polarized ERS populations in Fig. 3(b) for $S_{1.4\,\rm GHz} \leq 100$ mJy and Fig. 3(c) for $S_{1.4\,\rm GHz} > 100$ mJy.

For the polarized ERS with $S_{1.4\,\rm GHz} \leq 100$ mJy, Fig. 3(b), we have 98 *WISE*–AGN sources and 94 *WISE*–Star sources. We found the mean percentage polarization $\langle\Pi_{\rm AGN}\rangle = 6.7 \pm 0.2$ per cent for the *WISE*–AGN population and $\langle\Pi_{\rm Star}\rangle = 14.0 \pm 0.7$ per cent for our *WISE*–Star population. We did a Kolmogorov-Smirnov (KS) test of the percentage polarization of the two ERS populations and found that the two distributions are not drawn from the same parent population at the 99 per cent significance level.

For the polarized ERS with $S_{1.4\,\rm GHz} > 100$ mJy, Fig. 3(c), we have 1958 *WISE*–AGN sources and 172 *WISE*–Star sources. We found the mean percentage polarization $\langle\Pi_{\rm AGN}\rangle = 3.5 \pm 0.1$ per cent for the *WISE*–AGN population and $\langle\Pi_{\rm Star}\rangle = 7.7 \pm 0.5$ per cent for our *WISE*–Star population. We did a KS test of the percentage polarization of the two ERS populations and found that the two distributions are not drawn from the same parent population at the 99 per cent significance level.

4.2 Redshift distribution

Fig. 4 shows the redshift distribution of the two source populations as defined in Section 4.1. The polarized *WISE*–Star population are found to be low-redshift galaxies in the range $0.006 < z < 0.8$, while the polarized *WISE*–AGN population are high-redshift galaxies, and therefore more luminous, in the range $0.5 < z < 3.7$. We recognize that *WISE* is not sensitive to early-type galaxies at high redshift as they are too faint. Our sample of galaxies at high redshift must consist of luminous AGN or starburst or a mixed population of both.

4.3 1.4 GHz monochromatic luminosity distribution

The 1.4 GHz monochromatic luminosity ($L_{1.4\,\rm GHz}$) of the 4003 radio sources from the Hammond et al. (2012) catalogue was calculated using the equations of Hogg (1999):

$$L_{1.4\,\rm GHz} = \frac{4\pi D_{\rm L}^2 S_{1.4\,\rm GHz}}{(1+z)}(1+z)^{-\alpha}, \quad (6)$$

where $D_{\rm L}$ is the luminosity distance, $S_{1.4\,\rm GHz}$ is the flux density at 1.4 GHz, α the spectral index, and z is the redshift.

Spectral indices are required to calculate the monochromatic luminosity of the ERS. We calculated spectral indices from the 325 MHz Westerbork Northern Sky Survey (WENSS; Rengelink et al. 1997), which covers declinations $\geq 28\overset{\circ}{.}5$. WENSS has an angular resolution of 54 arcsec × 54 arcsec cosecδ and contains more than 200 000 sources down to a flux density of $S_{325\,\rm MHz} = 18$ mJy. Fig. 5 shows the distribution of spectral indices for the two *WISE* populations of polarized ERS. The median spectral index of polarized *WISE*–Star ERS ($N_{\rm Star} = 78$) is -0.59 ± 0.05, while the polarized *WISE*–AGN ERS ($N_{\rm AGN} = 731$) is -0.63 ± 0.02.

In Fig. 6, we plot the monochromatic luminosity of polarized ERS in the two *WISE* populations. The luminosity range of our full

[1] http://irsa.ipac.caltech.edu/Missions/wise.html

Table 2. Summary of key results from Section 4 for the two *WISE* populations of polarized ERS including: redshift range, median redshift, spectral index range, median spectral index, luminosity range, median angular and linear sizes, and RM. The errors in $\sigma_{\rm err}$ indicate the 1σ range.

Population	z	$\langle z \rangle$	α_{325}^{1400}	$\langle \alpha_{325}^{1400} \rangle$	$L_{1.4}$ (W Hz^{-1})
Full	$0.001 < z < 5.3$	0.78	$-2.62 < \alpha < 3.36$	-0.68 ± 0.02	$6 \times 10^{21} < L < 1 \times 10^{29}$
WISE–AGN	$0.500 < z < 3.7$	1.03	$-2.62 < \alpha < 3.01$	-0.63 ± 0.02	$9 \times 10^{23} < L < 7 \times 10^{28}$
WISE–Star	$0.006 < z < 0.8$	0.06	$-1.94 < \alpha < 1.50$	-0.59 ± 0.05	$6 \times 10^{21} < L < 7 \times 10^{25}$
Population	$\langle \theta_{\rm AS} \rangle$ (arcsec)	$\langle \theta_{\rm LS} \rangle$ (kpc)	$\sigma_{\rm ERS}$ (rad m^{-2})	$\sigma_{\rm err}$ (rad m^{-2})	
Full	37 ± 1	214 ± 5	$6.3 < \sigma_{\rm ERS} < 6.9$ ($\pm$>0.3)	10.3 ± 0.1	
WISE–AGN	34 ± 1	253 ± 8	$12.0 < \sigma_{\rm ERS} < 12.1$ ($\pm$>0.2)	$6.4 < \sigma_{\rm err} < 6.5 \pm 0.2$	
WISE–Star	58 ± 5	69 ± 8	$7.4 < \sigma_{\rm ERS} < 8.7$ ($\pm$>1.0)	$9.2 < \sigma_{\rm err} < 9.4 \pm 0.9$	

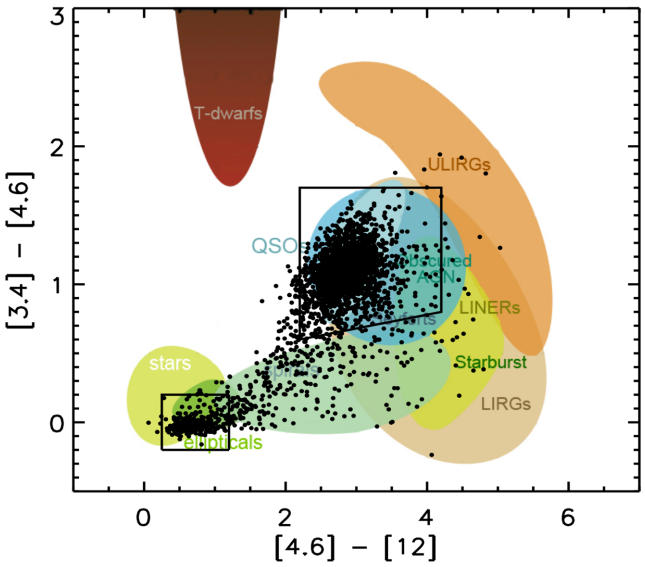

Figure 1. *WISE* colour–colour diagram, plotted in units of magnitude, for the polarized ERS with a 5σ detection in the three *WISE* bands of 3.4, 4.6, and 12 μm. The upper-right box indicates the region of *WISE*–AGN and the lower-left box indicates the region of *WISE*–Stars; all areas are described by Jarrett et al. (2011).

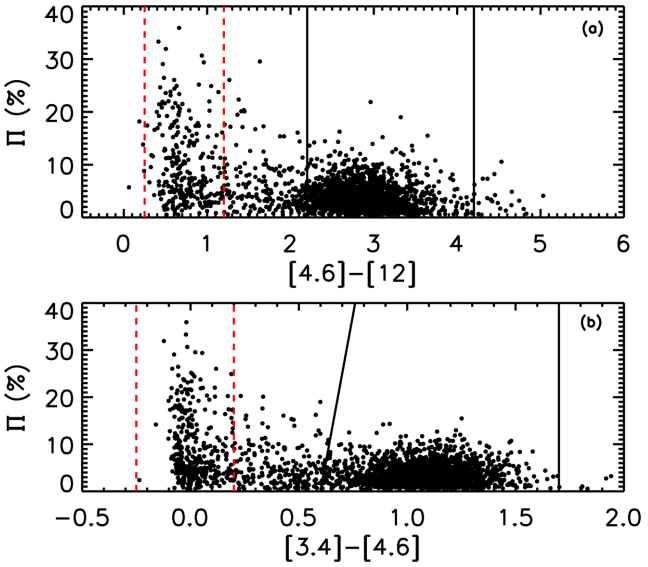

Figure 2. Percentage polarization as a function of *WISE* colour (a) [4.6] − [12] and (b) [3.4] − [4.6] from Fig. 1. The red dashed lines indicate the boundary of *WISE*–Star region and the solid black lines indicate the boundary of the *WISE*–AGN region as defined in Fig. 1.

sample of polarized ERS is $6 \times 10^{21} < L_{1.4\,\rm GHz} < 1 \times 10^{29}$ W Hz^{-1}, while for the *WISE*–AGN polarized ERS population the range is $9 \times 10^{23} < L_{1.4\,\rm GHz} < 7 \times 10^{28}$ W Hz^{-1}, and *WISE*–Star galaxies have $6 \times 10^{21} < L_{1.4\,\rm GHz} < 7 \times 10^{25}$ W Hz^{-1}. Our two *WISE* polarized ERS populations split into two separate regions around $L_{1.4\,\rm GHz} \sim 10^{25}$ W Hz^{-1} with the *WISE*–Star population filling out the lower luminosity side of the plot and the *WISE*–AGN population filling out the higher luminosity side of the plot. Following the relationship from Banfield et al. (2011), a power law of the form

$$\frac{\Pi}{\Pi_0} = \left(\frac{L_\nu}{L_0}\right)^\beta \tag{7}$$

was fit to the data. For the full sample of polarized ERS $\beta = -0.13 \pm 0.01$, for the *WISE*–AGN population $\beta = -0.08 \pm 0.01$ and $\beta = -0.29 \pm 0.05$ for the *WISE*–Star population. We ran a Spearman rank correlation test on the two population fits to determine the relationship between percentage polarization and monochromatic luminosity at 1.4 GHz. There is a moderate negative linear correlation for the *WISE*–Star population ($r_{s,\,\rm star} = -0.53 \pm 0.07$, $N_{\rm star} = 78$, $p < 0.01$) and a weak negative linear correlation for the *WISE*–AGN population ($r_{s,\,\rm AGN} = -0.24 \pm 0.02$, $N_{\rm AGN} = 731$, $p < 0.01$).

4.4 Rotation measures

In order to compare the extragalactic contributions to the RMs of the nearby *WISE*–Star sources and the distant *WISE*–AGN we have to correct for the RM contributions by the Galactic foreground and measurement errors. We follow the method described in Schnitzeler (2010) to correct for Galactic RM foregrounds, which separates Galactic from extragalactic RM contributions based on the idea that the former contributions are correlated between sightlines, while the latter are not. First we split the data into strips along Galactic longitude and use cubic spline fitting to remove large-scale RM gradients along Galactic longitude. The strips span only a narrow range in Galactic latitude to suppress the variation in Galactic RM with Galactic latitude. In Appendix A, we show how the measured RM variance of the ensemble after the cubic spline fitting can be written in terms of the RM variance that is built-up outside the Milky Way ($\sigma^2_{\rm ERS}$), the variance that is due to measurement errors ($\sigma^2_{\rm err}$), and a residual RM variance due to the Milky Way ($\sigma^2_{\rm MW}$) that

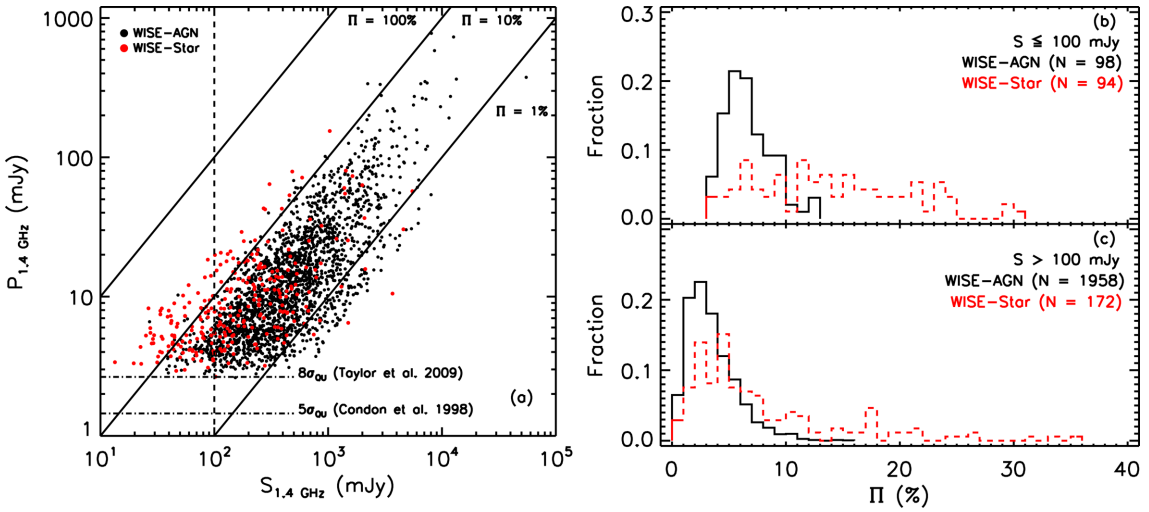

Figure 3. (a) Distribution of $\log(S_{1.4\,\mathrm{GHz}})$ versus $\log(P_{1.4\,\mathrm{GHz}})$ for the polarized ERS in Fig. 1. The red dots indicate the polarized ERS in the *WISE*–Star region, while the black dots indicate the polarized ERS in the *WISE*–AGN region. The solid diagonal lines indicate the $\Pi = 1$ (right), 10 (middle), and 100 per cent (left) percentage polarization levels. Also plotted are the $8\sigma_{\mathrm{QU}}$ flux density limit of the Taylor et al. (2009) catalogue and the $5\sigma_{\mathrm{QU}}$ flux density limit from NVSS (Condon et al. 1998). (b) Percentage polarization histogram of the fraction of polarized ERS in the *WISE*–AGN (black line) and *WISE*–Star (red line) regions for $S_{1.4\,\mathrm{GHz}} \leq 100$ mJy as indicated by the vertical dashed line in (a). (c) The same histogram as in (b) but for $S_{1.4\,\mathrm{GHz}} > 100$ mJy.

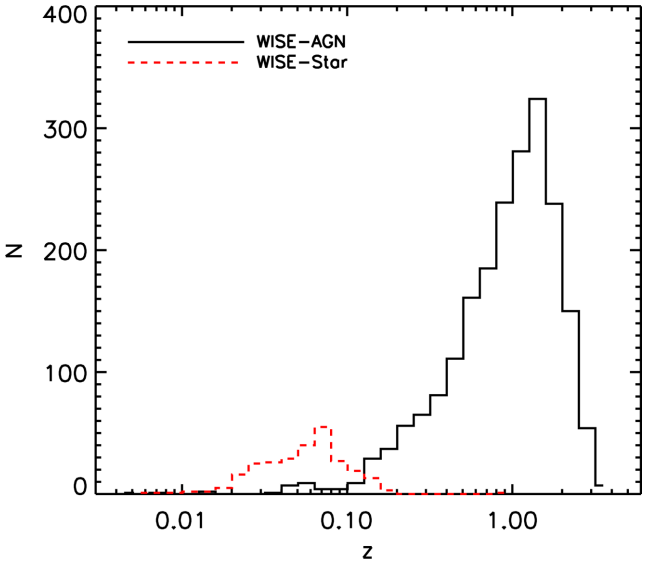

Figure 4. Redshift distribution of polarized ERS in the two regions defined in Fig. 1. The red dashed line represents the 266 polarized *WISE*–Star ERS. The black solid line represents the 2056 polarized *WISE*–AGN ERS.

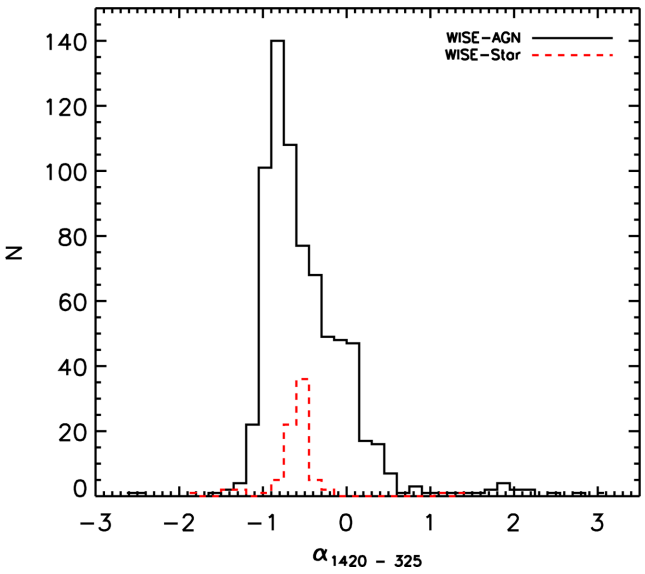

Figure 5. Spectral index distribution between 1400 and 325 MHz of the polarized ERS in our sample. The *WISE*–Star ERS is indicated by the red dashed line and the *WISE*–AGN ERS is given by the black solid line. The median spectral index for the *WISE*–Star population is -0.59 ± 0.05 and -0.63 ± 0.02 for the *WISE*–AGN polarized ERS population.

could not be removed as

$$\sigma^2_{\mathrm{RM}} = \left(\sigma^2_{\mathrm{ERS}} + \sigma^2_{\mathrm{err}}\right)\left(\frac{N_{\mathrm{los}} - N_{\mathrm{strips}}}{N_{\mathrm{los}} - 1}\right) + \sum_{\mathrm{strip}\ i=1}^{N_{\mathrm{strips}}} \frac{N_i}{N_{\mathrm{los}} - 1}\left(\langle \mathrm{RM}\rangle_{\mathrm{strip}\ i} - \langle \mathrm{RM}\rangle_{\mathrm{all\ strips}}\right)^2 + \sum_{\mathrm{strip}\ i=1}^{N_{\mathrm{strips}}}\left(\frac{N_i - 1}{N_{\mathrm{los}} - 1}\right)\sigma^2_{\mathrm{MW},i}, \quad (8)$$

where N_{los} is the total number of sightlines in the ensemble, N_{strips} is the total number of strips along Galactic longitude and N_i is the number of useable sightlines in strip i. $\langle \mathrm{RM}\rangle_{\mathrm{strip}\,i}$ and $\langle \mathrm{RM}\rangle_{\mathrm{all\ strips}}$ indicate the mean RM in a single strip and the mean RM of all sightlines combined, respectively. The strips in equation (8) are used to correct for the RM variance from the Milky Way that remains after cubic spline fitting (σ^2_{MW}); these strips do not have to be the same as the strips that we used for cubic spline fitting. In our analysis, we only use sightlines that lie further than 20° from the Galactic plane to avoid regions where the Galactic RM shows complex behaviour. We consider only sightlines if they belong to strips with at least 5–15 sightlines (i.e. polarized ERS) in them; we vary this number, and we vary the width of the strips between 5° and 15° in Galactic longitude to check how robust our results for σ^2_{ERS} are. If the number of sightlines in a strip is smaller than a specified minimum then all sightlines that belong to the strip are excluded from our analysis.

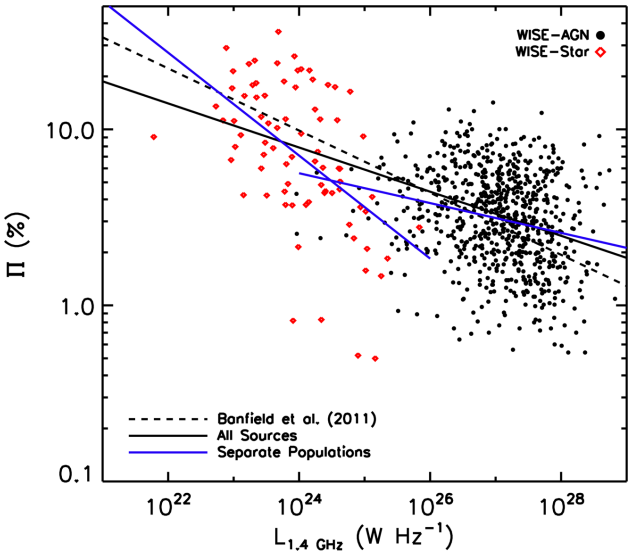

Figure 6. Percentage polarization versus luminosity for our sample of polarized ERS. The polarized *WISE*–AGN ERS are shown by the black dots, while the *WISE*–Star ERS are shown with red diamonds. A power law was fit to the full data set (solid black line), only to the *WISE*–AGN population (solid blue line on right), and only to the *WISE*–Star population (solid blue line on left). For comparison, the fit from Banfield et al. (2011) is shown as the black dashed line. For the full sample of polarized ERS $\beta = -0.13 \pm 0.01$, for the *WISE*–AGN population $\beta = -0.08 \pm 0.01$, and -0.29 ± 0.05 for the *WISE*–Star polarized ERS population.

The mean, standard deviation, and variance are calculated using robust statistics that reject outliers at the 3σ level.

We test our method using all sightlines and find $\sigma_{\rm ERS} = 6.7 - 6.9\,{\rm rad\,m^{-2}}$ ($\pm > 0.3\,{\rm rad\,m^{-2}}$). As we explain in Appendix A, we can calculate only a lower limit to the uncertainty in $\sigma_{\rm ERS}$. We then shift the strips by half a strip width to enable Nyquist sampling in Galactic latitude, and recalculate $\sigma^2_{\rm ERS}$, finding $\sigma_{\rm ERS} = 6.3 - 6.5\,{\rm rad\,m^{-2}}$. From a Monte Carlo simulation, we derive $\sigma_{\rm err} = 10.3 \pm 0.1\,{\rm rad\,m^{-2}}$ (1σ). Schnitzeler (2010) derived $\sigma_{\rm ERS} \approx 6\,{\rm rad\,m^{-2}}$ and $\sigma_{\rm err} = 10.4 \pm 0.4\,{\rm rad\,m^{-2}}$, in good agreement with the values we found.

The polarized ERS identified as *WISE*–AGN have $\sigma_{\rm ERS}$ between 12.0 and $12.1\,{\rm rad\,m^{-2}}$ ($\pm > 0.2\,{\rm rad\,m^{-2}}$), while $\sigma_{\rm err} = 6.4 - 6.5 \pm 0.2\,{\rm rad\,m^{-2}}$. The extragalactic RM variance of the *WISE*–AGN is considerably larger than the extragalactic RM variance of the ensemble of all sources. The RM variance of the ensemble can be written as a weighted mean of the RM variances of the subpopulations; our observation that the subpopulation of *WISE*–AGN sources has a much larger RM variance than the ensemble as a whole implies that the subpopulations must cover a wide range of RM variances. At different redshifts different subpopulations will contribute to the ensemble, which leads to a change in the RM variance in the ensemble as a function of redshift that could be misinterpreted as a signal from cosmological large-scale structure. Therefore, when studying cosmological RM contributions, one should try to understand the composition of the ensemble of sources from which the RM variance is calculated.

Because the number of *WISE*–Star sources is so much smaller than the number of *WISE*–AGN sources, strips that we use to correct for $\sigma^2_{\rm MW}$ often contain fewer *WISE*–Star sources than the required minimum number of sources. We also found that for a strip width of 5° the distribution of *WISE*–Star RMs could be non-Gaussian. To minimize the impact of these two effects, for *WISE*–Star sources we only use strip widths of 10° and 15°, and we found that $\sigma_{\rm ERS} = 7.4 - 8.7\,{\rm rad\,m^{-2}}$ ($\pm > 1.0\,{\rm rad\,m^{-2}}$) and $\sigma_{\rm err} = 9.2$–$9.4 \pm 0.9\,{\rm rad\,m^{-2}}$.

Based on the $\sigma_{\rm ERS}$ of the *WISE*–Star and the *WISE*–AGN sources we conclude that they are different at the ($\lesssim$) 4σ level. In Appendix A, we explain why the uncertainties in $\sigma_{\rm ERS}$ that we derive are lower limits, turning the statistical significance of the difference in $\sigma_{\rm ERS}$ between the two populations into an upper limit.

4.5 Polarized ERS angular and linear size distribution

Using the Faint Images of the Radio Sky at Twenty Centimetres (FIRST; White et al. 1997) survey, we determined the angular size for 2088 of our polarized ERS. We estimated the angular size by locating the 5σ boundary of the radio source and measuring the distance between boundary edges. The median angular size of the polarized *WISE*–Star ERS population is $\langle\theta_{\rm AS}\rangle = 58 \pm 1$ arcsec and for the polarized *WISE*–AGN ERS population $\langle\theta_{\rm AS}\rangle = 34 \pm 1$ arcsec. Both populations are resolved in FIRST ($\theta \sim 5$ arcsec), consistent with polarized radio sources being resolved lobe-dominated sources (Grant et al. 2010). Our findings are consistent with Rudnick & Owen (2014) who found a small fraction of their polarized sources with angular sizes >50 arcsec. In Fig. 7, we plot the angular size distribution with total flux density and percentage polarization distribution for the two separate *WISE* polarized ERS populations. The polarized ERS were binned so that each bin contained roughly the same number of sources, and the median value of the angular size was determined for each bin. The median values for the *WISE*–Star population are indicated by red stars in Fig. 7, while the *WISE*–AGN population median angular size values are plotted with black dots. There is a separation in the median angular sizes between the two *WISE* polarized ERS populations, with the *WISE*–Star population having larger angular sizes than the *WISE*–AGN population. We note that the median angular sizes do not change significantly with percentage polarization and total flux density for both populations.

We investigated the effect of resolution by comparing the percentage polarization of sources resolved in NVSS, $\theta_{\rm AS} \geq 45$ arcsec, and those unresolved in NVSS, $\theta_{\rm AS} < 45$ arcsec. For the polarized ERS resolved in NVSS, we find that the *WISE*–AGN polarized ERS have a median angular size of 55 ± 1 arcsec and a median percentage polarization of 3.6 ± 0.2 per cent, while the *WISE*–Star polarized ERS are larger with a median angular size of 66 ± 3 arcsec and a median percentage polarization of 6.3 ± 0.9 per cent. For our sources that are unresolved in NVSS we find that the *WISE*–AGN

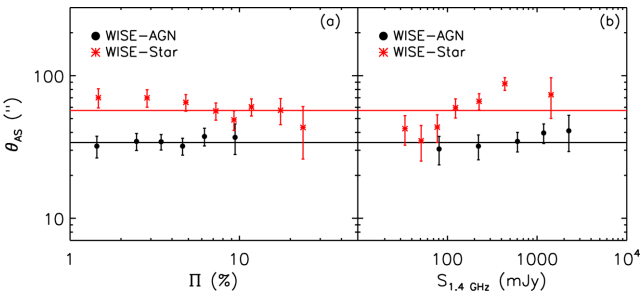

Figure 7. (a) Distribution of median angular size as a function of percentage polarization for the two *WISE* polarized ERS populations. (b) Distribution of median angular size as a function of total flux density for the two *WISE* polarized ERS populations. The *WISE*–AGN population is shown with black dots and the *WISE*–Star population is shown with red stars. The errors bars are the standard error on the mean. The median angular size of the two populations is shown with the solid lines.

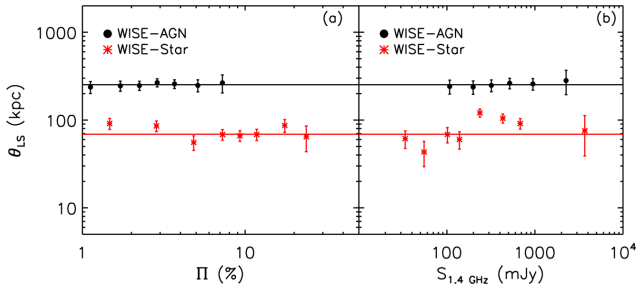

Figure 8. (a) Distribution of median linear size as a function of percentage polarization for the two *WISE* polarized ERS populations. (b) Distribution of median linear size as a function of total flux density for the two *WISE* polarized ERS populations. The *WISE*–AGN population is shown with black dots and the *WISE*–Star population is shown with red stars. The errors bars are the standard error on the mean. The median linear size of the two populations is shown with the solid lines.

polarized ERS have a median angular size of 31 ± 1 arcsec and a median percentage polarization of 3.3 ± 0.1 per cent, while the *WISE*–Star polarized ERS are larger with a median angular size of 35 ± 1 arcsec and a median percentage polarization of 9.5 ± 1.4 per cent. The percentage polarization for the *WISE*–AGN and *WISE*–Star populations is constant for the two angular size bins.

In Fig. 8, we plot the linear size of both classifications of polarized ERS as a function of percentage polarization and total flux density. We calculated the linear size of the polarized ERS using the method outlined by Hogg (1999). The polarized *WISE*–AGN ERS population tends to be larger in linear size compared to the polarized *WISE*–Star ERS population. We have also plotted the median linear size values for the *WISE*–AGN population (black dots) and the *WISE*–Star (red stars) populations. Our two polarized ERS populations show a large difference in linear size. The median linear size of the *WISE*–AGN population is $\theta_{LS} = 253 \pm 8$ kpc and for the *WISE*–Star population 69 ± 8 kpc. We note that the median linear size value remains constant for both populations as a function of both percentage polarization and total flux density.

5 SELECTION EFFECTS

We acknowledge that there are selection effects with our polarized ERS populations and we discuss each briefly.

(1) *WISE* detections: *WISE* was built to survey the entire sky in the mid-infrared. As a result, *WISE* will observe the full extent of the obscured AGN and QSO and detect the ultraluminous infrared galaxies (Wright et al. 2010). However, *WISE* is not sensitive to elliptical or lenticular galaxies at high redshifts as these types of galaxies contain little dust and gas and will fall below the detection threshold of *WISE*. Elliptical galaxies are known to host powerful AGN so our sample of polarized *WISE*–Star sources is biased towards low redshift, whereas our sample of *WISE*–AGN sources will be detectable out to $z = 3$ (Wright et al. 2010). We also note that highly luminous quasar-like galaxies are rare at low redshift and as a result of these effects our two populations of polarized ERS do not overlap significantly in redshift space, see Fig. 4.

(2) Redshift selection: the Hammond et al. (2012) catalogue contains redshifts from various optical surveys with different sensitivity limits as mentioned in Section 3.1. A number of high-redshift AGN will not be detected in these surveys as the optical host galaxy is fainter than their counterpart at low redshift. Therefore, the Hammond et al. (2012) catalogue will be biased towards optically brighter and more nearby AGN.

(3) Polarized flux density detection limit: in all polarization studies there is a bias towards high percentage polarization near the detection limit of the images. We see this bias in our sample (Fig. 6) where there is a shortage of polarized ERS with $\Pi \leq 3$ per cent at $L_{1.4\,GHz} \leq 10^{25}$ W Hz^{-1}. Both the *WISE*–AGN and *WISE*–Star ERS suffer from selection effects in the same way. There are no highly polarized *WISE*–AGN at $S_{1.4\,GHz} \leq 100$ mJy in Fig. 3(a) which, if there are any, should have been detected. Instead, we only detect highly polarized *WISE*–Star ERS at these flux density levels.

Although *WISE* is sensitive to certain types of galaxies, we find that our sample splits nicely into two separate host galaxy populations as shown in Fig. 1 and with this split we analyse the properties of both samples. We acknowledge that our sample is not statistically complete and that we may be affected by unknown selection effects not mentioned above. We notice this possibility in the fact that our mean Π for both populations is higher than estimated by both Mesa et al. (2002) and Tucci et al. (2004). We also notice in both Figs 3(a) and 6 that there is a lack of highly polarized *WISE*–AGN sources across all flux densities whereas the *WISE*–Star population begins to fill out this area at $S_{1.4\,GHz} \leq 100$ mJy regardless of the fact that only highly polarized sources are detected at the faint flux density levels. The fact that we do not detect the *WISE*–AGN with high percentage polarization at $S_{1.4\,GHz} \leq 100$ mJy demonstrates a change in the intrinsic properties of polarized ERS as the percentage polarization is greater for *WISE*–Star than for *WISE*–AGN at these flux densities. In the next section we discuss possible astrophysical reasons for our findings noting these selection effects in our data.

6 DISCUSSION

6.1 Is the polarization correlation with flux real?

Mesa et al. (2002) and Tucci et al. (2004) found an inverse correlation between the percentage linear polarization and total flux densities of NVSS sources, so that faint sources were more highly polarized. A similar result was found for the European Large Area *ISO* Survey North 1 field (ELAIS-N1) sources by Taylor et al. (2007) and Grant et al. (2010), and for the Australia Telescope Low-brightness Survey (ATLBS) sources by Subrahmanyan et al. (2010). Rudnick & Owen (2014) show that the Grant et al. (2010) completeness correction is too large at the faintest polarized flux density bins but they also come to the conclusion that the population of polarized radio sources changes in composition.

However, Hales (2013), while finding an observational increase in percentage polarization with decreasing flux density in the ATLAS data set, attributed this entirely to selection effects, including the non-detections which must be accounted for in a full statistical treatment. Once the data were corrected for these effects, Hales (2013) found that the percentage polarization of their sources showed no dependence on flux density, agreeing with results at higher frequencies by Massardi et al. (2013). These results cast doubt on earlier results that had found such dependence.

We show that the correlation between percentage polarization and flux density is real and cannot be the result of selection effects. Fig. 3 shows that sources with a *WISE* classification of star (i.e. passive and quiescent galaxies) show an increase in fractional polarization with decreasing flux density, while a weaker trend is found for sources with a *WISE* classification of AGN (i.e. luminous quasar-like galaxies). Selection effects in total flux density affect both the *WISE*–Star and *WISE*–AGN populations at low total flux density and polarized flux density. If the overall increase with

percentage polarization with decreasing flux density were due to bias or selection effects in the radio data, then, for a given radio flux density or percentage polarization, these effects would show no correlation with *WISE* colours. This is inconsistent with Figs 2 and 3, which demonstrate that the percentage polarization depends on *WISE* colours.

Given that the effect is demonstrably present in our data set, we can then examine why Hales (2013) failed to detect it after removing selection effects. Data from Hales (2013) probe much lower radio flux densities, so probe much larger redshift range, over a much smaller area than our data set. Since quiescent galaxies result from hierarchical merging of star-forming galaxies, they are less numerous at high redshift than at low redshift. It is therefore likely that the data from Hales (2013) include a smaller number of *WISE*–Star galaxies, and so the trend we see here will be very much reduced in the Hales (2013) data set. If this explanation is correct, then the inconsistency between Hales (2013) and other authors is an indication not of problems with the data, but of cosmic evolution of the space density of quiescent galaxies. This will be investigated further in the ATLAS Data Release 3 by Banfield et al. (in preparation).

6.2 The origin of the polarization correlation with flux

Shi et al. (2010) and Banfield et al. (2011) conclude that the inverse correlation of percentage polarization and total flux density may be a result of the intrinsic properties of the polarized ERS. Using ERS with $\Pi > 30$ per cent, Shi et al. (2010) show that polarized ERS at 1.4 GHz are contained within elliptical galaxies and that there is no dependence on the source environment compared to low polarization ERS. Banfield et al. (2011) confirmed that there is no trend of percentage polarization with redshift, however, a trend of increasing percentage polarization with decreasing luminosity was found. Hammond et al. (2012) found that polarized ERS with optical counterparts classified as galaxies have higher polarization percentages compared to polarized ERS with optical classifications as quasars, agreeing that a population change in polarized ERS may be the cause of the inverse correlation between percentage polarization and total flux density.

Our sample of polarized ERS shows a strong distinction between two different galaxy populations. The two populations differ in both infrared colours and radio polarization properties. The *WISE*–AGN ERS are radio-loud AGN at high radio luminosity and have larger linear sizes compared to the *WISE*–Star ERS. The infrared emission from the *WISE*–AGN can originate from dust that is being heated by some combinations of AGN and star formation activity. The *WISE*–Star ERS are also radio-loud AGN at lower radio luminosity and have smaller linear sizes. The infrared emission from the *WISE*–Star originates from the stars within the galaxy, pointing to an old elliptical galaxy. The *WISE*–AGN population show lower percentage polarization than the *WISE*–Star population.

Our results confirm the previous by Taylor et al. (2007), Banfield et al. (2011), and Hammond et al. (2012) that the percentage polarization increases with decreasing total flux density is the result of a population change. Our sample of highly polarized ERS is found to be part of the *WISE*–Star population, endorsing the result from Shi et al. (2010) that the polarized radio sources are inside elliptical galaxies. Since Hales (2013) find no such trend after removing selection effects, we conclude that the Hales (2013) data set contain fewer *WISE*–Star ERS. Further investigation is required to determine if there is an evolution of one population of polarized ERS to another population of polarized ERS.

6.3 Environments of polarized radio sources

High-redshift radio galaxies (HzRGs; Seymour et al. 2007; De Breuck et al. 2010) are radio galaxies found at $1 < z < 5$ and are indicators of large overdensities or protoclusters in the early Universe (Miley & De Breuck 2008). Our sample of polarized *WISE*–AGN lie between $z = 0.5$ and 3.7 with luminosities in the range of $9 \times 10^{23} < L_{1.4} < 7 \times 10^{28}$ W Hz^{-1}; placing our sources in the category of HzRGs. Humphrey et al. (2013) provide evidence that HzRGs in these over dense regions can be surrounded by giant ionized gas haloes. Radio observations of Cygnus A by Dreher, Carilli & Perley (1987) revealed large fluctuations in RM across the lobes and magnetic field reversals of the order of ∼20 kpc. Dreher et al. (1987) suggest that the intracluster medium (ICM) or a sheath surrounding the radio lobes can cause these high RMs. Models by Bicknell, Cameron & Gingold (1990) suggest a turbulent interface between the magnetised plasma in the radio lobe and the ICM causing reversals in the magnetic field. Recent observations of Centaurus A by O'Sullivan et al. (2013) provide evidence of depolarization across radio lobes from the presence of a significant amount of thermal gas within the lobes. Bell & Comeau (2013) examine a sample of radio sources exhibiting the Laing-Garrington effect and show that the depolarization cannot be explained by beaming. Farnes, Gaensler & Carretti (2014) compared total intensity spectral indices with polarized spectral indices to show that there are two populations of polarized radio sources: core- and jet-dominated sources. Farnes et al. (2014) suggest that these two different source populations undergo different depolarization mechanisms based on the local source environment. Our work supports the conclusions from other authors that *WISE*–AGN have larger linear sizes consistent with being more powerful and lower percentage polarization. As the radio galaxy expand through the over dense regions surrounding the host galaxy, mixing between the radio lobes and the surrounding gas tangles the magnetic field line, which results in depolarization.

6.4 Extragalactic rotation measures

The *WISE*–Star and *WISE*–AGN populations have different RM variances, which is a combination of the different physical properties of these radio sources (star-forming galaxies versus AGN) and from the longer lines of sight towards the *WISE*–AGN sources, which can host more intervening objects that leave their imprint on the RMs of the background sources. We write the extragalactic RM contributions that we find after removing the Galactic foreground contribution as

$$\mathrm{RM} = \mathrm{RM}_{\mathrm{MW,res}} + \mathrm{RM}_{\mathrm{web}} + \mathrm{RM}_{\mathrm{cluster}} + \mathrm{RM}_{\mathrm{Mg\,II}} + \frac{\mathrm{RM}_{\mathrm{int}}}{(1+z)^2} + \mathrm{rest}, \quad (9)$$

which decomposes the extragalactic RM into contributions by the Milky Way that have not been completely removed, intervening structures in the cosmic web, galaxy clusters, and Mg II absorbers, the source-intrinsic RMs corrected for their redshift, z, and a rest term which we will show plays only a very small role. Assuming that the RMs in equation (9) follow Gaussian distributions, the RM variances can be written as

$$\sigma^2_{\mathrm{RM}} = \sigma^2_{\mathrm{RM,MW_{res}}} + \sigma^2_{\mathrm{RM,web}} + \sigma^2_{\mathrm{RM,cluster}} + \sigma^2_{\mathrm{RM,Mg\,II}} + \frac{\sigma^2_{\mathrm{RM,int}}}{(1+z)^4} + \sigma^2_{\mathrm{rest}}. \quad (10)$$

Here we used $\langle \mathrm{RM_{MW,\,res}} \rangle \approx 0\,\mathrm{rad\,m^{-2}}$ from our simulations, and the fact that the net RMs in intervening objects are zero on average. While clusters can have a considerable impact on the RM variance of background sources (e.g. Clarke 2004), Johnston-Hollitt & Grimwood (2011) showed that the mean RM of sources from the NVSS catalogue that lie behind clusters is $\approx 0\,\mathrm{rad\,m^{-2}}$.

From the simulations by Akahori & Ryu (2011) and the observations by Joshi & Chand (2013) we can estimate the contributions by cosmological large-scale structure and intervening Mg II absorbers, respectively, on the extragalactic RM variances that we observed. While some of Mg II absorption can be associated with the host quasars (e.g. Farina et al. 2014) or host galaxies (e.g. Bordoloi et al. 2014) themselves, in our analysis we should only correct for the contribution by intervening Mg II absorbers that are not associated with the host quasars or galaxies. In their study of the RM imprint of intervening Mg II absorbers, Joshi & Chand (2013) considered only Mg II absorbers with relative velocities of more than 5000 km $\mathrm{s^{-1}}$ with respect to the background quasars. We estimate the contribution by intervening Mg II absorbers to the σ_{RM} we derived based on this analysis by Joshi & Chand (2013) of intervening Mg II systems.

For the high-redshift *WISE*–AGN (median redshift of 1.02) large-scale structure contributes 7–8 $\mathrm{rad\,m^{-2}}$. Models 'ALL' and 'CLS' from Akahori & Ryu (2011) predict larger standard deviations in RM, but contain contributions by galaxy clusters that could not be properly modelled given the cell size of the simulations, as the authors mention in their Section 2.2. Joshi & Chand (2013) found that sightlines with Mg II absorbers show an increase in the standard deviations in RM by $8.1 \pm 4.8\,\mathrm{rad\,m^{-2}}$, and that about 1/3 of the sightlines towards high-redshift sources contain one or more Mg II absorbers. Combining the increased RM variance due to intervening Mg II absorbers with the frequency with which such systems are encountered gives $\sigma^2_{\mathrm{RM,Mg\,II}} = 18.4\,(\mathrm{rad\,m^{-2}})^2$. For the low-redshift *WISE*–Star sources (median redshift of 0.06) large-scale structure contributes $\approx 1.4\,\mathrm{rad\,m^{-2}}$, and we assume that the contribution by Mg II absorbers is negligible given the short sightlines towards the *WISE*–Star sources.

With this information we can write out equation (10) separately for the low-redshift *WISE*–Star sources and the high-redshift *WISE*–AGNs, and subtract the two expressions. Using the RM variances that we derived for the *WISE*–Star and *WISE*–AGN samples that we determined in Section 4.4, one can show that

$$\left(\sigma^2_{\mathrm{RM,cluster}} + \frac{\sigma^2_{\mathrm{RM,int}}}{(1+z)^4}\right)_{z\approx 1} = \left(\sigma^2_{\mathrm{RM,cluster}} + \frac{\sigma^2_{\mathrm{RM,int}}}{(1)^2}\right)_{z\approx 0} + 8\,(\mathrm{rad\,m^{-2}})^2, \quad (11)$$

where the numerical term was calculated as 144-64-18-(56-2) $(\mathrm{rad\,m^{-2}})^2$, combining the extragalactic RM variances of the high-redshift *WISE*–AGNs and low-redshift *WISE*–Star sources, and the contribution by the cosmic web and Mg II absorbers. Given the very different physical properties of the *WISE*–AGN and *WISE*–Star sources, which are reflected in $\sigma_{\mathrm{RM,\,int}}$, and the contributions by clusters that we could not estimate, the 'excess' of 8 $(\mathrm{rad\,m^{-2}})^2$ in the variance is very small. This excess includes the difference in residual contributions by the Milky Way for the *WISE*–AGN and *WISE*–Star sources, and contributions by sources along the line of sight that we included as the rest term in equations (9) and (10).

Long lines of sight have a higher chance of passing through galaxy clusters than short lines of sight, and as a result, $(\sigma^2_{\mathrm{RM,cluster}})_{z\approx 1} > (\sigma^2_{\mathrm{RM,cluster}})_{z\approx 0}$. Therefore, equation (11) also implies that the distribution of the source-intrinsic RMs of the *WISE*–AGN, measured in terms of the standard deviation, is at most four times as wide as the distribution of RMs of the *WISE*–Star star-forming galaxies, if the standard deviation of the *WISE*-Star galaxies itself is not too small.

7 CONCLUSIONS

Using the Hammond et al. (2012) catalogue of Faraday RMs and redshifts for 4003 ERS detected at 1.4 GHz, we have shown that polarized radio sources split into two types of host galaxies at two separate redshift ranges, as such the two populations are investigated separately and a larger sample of polarized radio sources is required to examine if one population evolves into the other population. We find the following:

(1) the anticorrelation between percentage polarization and total flux density is real as the percentage polarization depends on *WISE* mid-infrared colour;

(2) the polarized ERS separate clearly into two infrared-selected objects: *WISE*–Star sources that are low-redshift, low-radio-luminosity elliptical galaxies, and *WISE*–AGN which are high-redshift, high-radio-luminosity quasar-like galaxies;

(3) our sample has a larger number of quiescent galaxies than Hales (2013), suggesting that the inconsistency between the data sets is an indication of cosmic evolution of the space density of quiescent galaxies;

(4) we suggest that the difference in the percentage polarization of radio galaxies originates from the environment of the host galaxy. Our *WISE*–AGN population is consistent with HzRGs in denser environments where depolarization is more severe compared to the *WISE*–Star sources that are not very active;

(5) we find that the extragalactic RM contributions to the nearby *WISE*–Star and the distant *WISE*–AGN sources are different; the distribution of source-intrinsic RMs of the *WISE*–AGNs is at most four times as wide as the distribution of intrinsic RMs of the star-forming *WISE*–Star galaxies if the distribution of intrinsic RMs of the *WISE*–Star sources itself is at least several $\mathrm{rad\,m^{-2}}$ wide; and

(6) we also detect no evolution of RM with redshift, suggesting that the RM is a product of the intrinsic properties of the radio galaxy and not a result of the intervening large-scale structure of the Universe.

ACKNOWLEDGEMENTS

The authors would like to thank H-R. Klöckner for his useful comments on the manuscript, B. M. Gaensler for his advice on the rotation measure catalogue, L. Rudnick for the discussion on rotation measures and polarized source populations, and the anonymous referee for the suggestions making our paper stronger. This publication makes use of data products from the *Wide-field Infrared Survey Explorer*, which is a joint project of the University of California, Los Angeles, and the Jet Propulsion Laboratory/California Institute of Technology, funded by the National Aeronautics and Space Administration. This publication makes use of data products from the Sloan Digital Sky Survey. Funding for the SDSS and SDSS-II has been provided by the Alfred P. Sloan Foundation, the Participating Institutions, the National Science Foundation, the US Department of Energy, the National Aeronautics and Space Administration, the Japanese Monbukagakusho, the Max Planck Society, and the Higher Education Funding Council for England. The SDSS website is http://www.sdss.org.

REFERENCES

Akahori T., Ryu D., 2011, ApJ, 738, 134
Banfield J. K., George S. J., Taylor A. R., Stil J. M., Kothes R., Scott D., 2011, ApJ, 733, 69
Bell M. B., Comeau S. P., 2013, Ap&SS, 344, 205
Bicknell G. V., Cameron R. A., Gingold R. A., 1990, ApJ, 357, 373
Borodoli R., Lilly S. J., Kacprzak G. G., Churchill C. W., 2014, ApJ, 784, 108
Clarke T. E., 2004, J. Korean Astron. Soc., 37, 337
Colless M. et al., 2001, MNRAS, 328, 1039
Condon J. J., Cotton W. D., Greisen E. W., Yin Q. F., Perley R. A., Taylor G. B., Broderick J. J., 1998, AJ, 115, 1693
Croom S. M., Smith R. J., Boyle B. J., Shanks T., Miller L., Outram P. J., Loaring N. S., 2004, MNRAS, 349, 1397
De Breuck C. et al., 2010, ApJ, 725, 36
Dreher J. W., Carilli C. L., Perley R. A., 1987, ApJ, 316, 611
Fanaroff B. L., Riley J. M., 1974, MNRAS, 167, 31
Farina E. P., Falomo R., Scarpa R., Decarli R., Treves A., Kotilainen J. K., 2014, MNRAS, 441, 886
Farnes J. S., Gaensler B. M., Carretti E., 2014, ApJS, 212, 15
George S. J., Stil J. M., Keller B. W., 2012, PASA, 29, 214
Grant J. K., Taylor A. R., Stil J. M., Landecker T. L., Kothes R., Ransom R. R., Scott D., 2010, ApJ, 714, 1689
Hales C. A., 2013, PhD thesis, Univ. Sydney
Hammond A. M., Robishaw T., Gaensler B. M., 2012, preprint (arXiv:1209.1438)
Helou G., Madore B. F., Schmitz M., Bicay M. D., Wu X., Bennett J., 1991, Databases On-line Data Astron., 171, 89
Hogg D. W., 1999, preprint (arXiv:9905116)
Humphrey A., Binette L., Villar-Martín M., Aretxaga I., Papaderos P., 2013, MNRAS, 428, 563
Jarrett T. H. et al., 2011, ApJ, 735, 112
Johnston-Hollitt M., Grimwood G., 2011, J. Astrophys. Astron., 32, 539
Jones D. H. et al., 2009, MNRAS, 399, 683
Joshi R., Chand H., 2013, MNRAS, 434, 3566
Massardi M. et al., 2013, MNRAS, 436, 2915
Mesa D., Baccigalupi C., De Zotti G., Gregorini L., Mack K.-H., Vigotti M., Klein U., 2002, A&A, 396, 463
Miley G., De Breuck C., 2008, A&AR, 15, 67
Morrison G. E., Owen F. N., Dickinson M., Ivison R., Ibar E., 2010, ApJS, 188, 178
O'Sullivan S. P. et al., 2013, ApJ, 764, 162
Rengelink R. B., Tang Y., de Bruyn A. G., Miley G. K., Bremer M. N., Roettgering H. J. A., Bremer M. A. R., 1997, A&AS, 124, 259
Rudnick L., Owen F. N., 2014, ApJ, 785, 45
Sadler E. M. et al., 2006, MNRAS, 371, 898
Schnitzeler D. H. F. M., 2010, MNRAS, 409, L99
Seymour N. et al., 2007, ApJS, 171, 353
Shi H., Liang H., Han J. L., Hunstead R. W., 2010, MNRAS, 409, 821
Simmons J. F. L., Stweart B. G., 1985, A&A, 142, 100
Sotomayor-Beltran C. et al., 2013, A&A, 552, 58
Stern D. et al., 2012, ApJ, 753, 30
Subrahmanyan R., Ekers R. D., Saripalli L., Sadler E. M., 2010, MNRAS, 402, 2792
Taylor A. R. et al., 2007, ApJ, 666, 201
Taylor A. R., Stil J. M., Sunstrum C., 2009, ApJ, 702, 1230
Tucci M., Toffolatti L., 2012, Adv. Astron., 2012, 52
Tucci M., Martínez-González E., Toffolatti L., González-Nuevo J., De Zotti G., 2004, New Astron. Rev., 47, 1135
Wardle J. F. C., Kronberg P. P., 1974, ApJ, 194, 249
Wenger M. et al., 2000, A&AS, 143, 9
White R. L., Becker R. H., Helfand D. J., Gregg M. D., 1997, ApJ, 475, 479
Wright E. L. et al., 2010, AJ, 140, 1868
York D. G. et al., 2000, AJ, 120, 1579

APPENDIX A: DERIVATION OF EXTRAGALACTIC ROTATION MEASURES

Consider a population of polarized ERS where each source has a RM. This RM contains contributions from all along the sight: the intrinsic RMs of the sources themselves, intergalactic space, the Milky Way, and the Earth's ionosphere. The RMs that are built-up inside and outside the Milky Way are much larger than the ionospheric RM (Sotomayor-Beltran et al. 2013). Using the RM values from the catalogue by Taylor et al. (2009), Schnitzeler (2010) has shown that the RM contribution by the Galactic foreground can be separated from the contribution from outside the Milky Way because the foreground RM contributions are correlated between sightlines, while the latter does not depend on the viewing direction in the Milky Way. Here we describe a simple method to calculate the extragalactic RM variance of the radio sources. First, we analyse how the RMs from different parts of the line of sight contribute to the RM variance that we measure for an ensemble of extragalactic sources, then we outline a five-step method to calculate the extragalactic RM variance of this ensemble. Similar to Schnitzeler (2010), we only include sightlines that lie further than 20° from the Galactic plane.

We use cubic spline fitting as described in Schnitzeler (2010) to remove large-scale RM gradients along Galactic longitude that are induced by the Milky Way. All RMs from the catalogue by Taylor et al. (2009) are included in this cubic spline fitting, also when we analyse the *WISE*–AGN and *WISE*–Star subpopulations. The strips that we use to fit and remove a cubic spline are 4° wide in Galactic latitude. We also calculate and remove a cubic spline fit to strips that are shifted by 2° (half a strip width) to provide Nyquist sampling of all Galactic latitudes.

The observed RM of a radio source can be split into a contribution by the Milky Way, a contribution from outside the Milky Way, and the measurement error in RM as

$$\mathrm{RM_{obs}} = \mathrm{RM_{MW}} + \mathrm{RM_{ERS}} + \mathrm{RM_{err}}. \tag{A1}$$

After cubic spline fitting, the variance of an ensemble of sightlines in a single strip along Galactic longitude can be written as

$$\sigma^2_{\mathrm{RM}} = \sigma^2_{\mathrm{MW}} + \sigma^2_{\mathrm{ERS}} + \sigma^2_{\mathrm{err}}, \tag{A2}$$

since the contributing RMs all have the same mean value (of 0 rad m^{-2}). This ensemble can be a subset from the catalogue by Taylor et al. (2009). When multiple strips are combined the variance of the ensemble of sightlines can be written as

$$\begin{aligned}
\sigma^2_{\mathrm{RM}} &= \frac{1}{N_{\mathrm{los}}-1}\sum_{i=1}^{N_{\mathrm{los}}}(\mathrm{RM_{obs}} - \langle\mathrm{RM}\rangle_{1+\cdots+M})^2 \\
&= \frac{N_1-1}{N_{\mathrm{los}}-1}\frac{1}{N_1-1}\sum_{\text{strip }1}(\mathrm{RM_{obs}} - \langle\mathrm{RM}\rangle_{\text{strip }1})^2 \\
&\quad + \cdots \\
&\quad + \frac{N_M-1}{N_{\mathrm{los}}-1}\frac{1}{N_M-1}\sum_{\text{strip }M}(\mathrm{RM_{obs}} - \langle\mathrm{RM}\rangle_{\text{strip }M})^2 \\
&\quad + \frac{N_1}{N_{\mathrm{los}}-1}\left(\langle\mathrm{RM}\rangle_{\text{strip }1} - \langle\mathrm{RM}\rangle_{1+\cdots+M}\right)^2 \\
&\quad + \cdots \\
&\quad + \frac{N_M}{N_{\mathrm{los}}-1}\left(\langle\mathrm{RM}\rangle_{\text{strip }M} - \langle\mathrm{RM}\rangle_{1+\cdots+M}\right)^2,
\end{aligned} \tag{A3}$$

if $N_{\rm los}$ sightlines are distributed over M strips. $N_{\rm los} = N_1 + \cdots + N_M$, where N_i is the number of sightlines in strip i. $\langle {\rm RM} \rangle_{1\,+\,\cdots\,+\,M}$ and $\langle {\rm RM} \rangle_{{\rm strip}\,i}$ indicate the mean RM of the ensemble of all strips and the mean RM of all sightlines in a single strip, respectively. Using equation (A2) to re-write equation (A3), and combining the $\sigma^2_{\rm ERS}$ and $\sigma^2_{\rm err}$ terms from the different strips, equation (A3) can be written as (equation 8 in text)

$$\begin{aligned}\sigma^2_{\rm RM} = {} & \left(\sigma^2_{\rm ERS} + \sigma^2_{\rm err}\right)\left(\frac{N_{\rm los} - N_{\rm strips}}{N_{\rm los} - 1}\right) \\ & + \frac{N_1 - 1}{N_{\rm los} - 1}\sigma^2_{{\rm MW},1} + \cdots + \frac{N_M - 1}{N_{\rm los} - 1}\sigma^2_{{\rm MW},M} \\ & + \frac{N_1}{N_{\rm los} - 1}\left(\langle {\rm RM}\rangle_{{\rm strip}\ 1} - \langle {\rm RM}\rangle_{1+\cdots+M}\right)^2 \\ & + \cdots \\ & + \frac{N_M}{N_{\rm los} - 1}\left(\langle {\rm RM}\rangle_{{\rm strip}\ M} - \langle {\rm RM}\rangle_{1+\cdots+M}\right)^2, \end{aligned} \tag{A4}$$

if there are $N_{\rm strips}$ with usable sightlines.

Using equation (A4) we can calculate the variance of the extragalactic RMs of the radio sources in the following way:

(1) calculate $\sigma^2_{\rm RM}$ for the ensemble of all sightlines after large-scale RM gradients have been removed by cubic spline fitting, then (working from right to left in equation A4)

(2) correct for the difference between the mean RM of the ensemble of all sightlines and the mean RM of sightlines belonging to a single strip,

(3) subtract the contribution by the Milky Way,

(4) divide by the bias-correction term, and

(5) subtract the variance in RM that is expected purely due to the measurement errors of the RMs.

The mean RM of individual strips and of the ensemble of all sightlines was found using robust statistics, where RM outliers at the 3σ level were removed from the ensemble.

Schnitzeler (2010) found that the Milky Way contributes $\sigma_{\rm RM,\,MW} = 6.8\,{\rm rad\,m^{-2}}/\sin({\rm latitude})$ at positive Galactic latitudes and $\sigma_{\rm RM,\,MW} = 8.4\,{\rm rad\,m^{-2}}/\sin(-{\rm latitude})$ at negative Galactic latitudes. To correct for how these contributions change with Galactic latitude we bin the ensemble of sightlines into strips along Galactic longitude; the width of these strips does not have to be the same as the width that we used to remove large-scale RM gradients by cubic spline fitting. In our analysis, we only used sightlines from a strip if the number of sightlines in that strip is larger than a threshold value. We varied both the strip width and the threshold value to check how robust our results are.

The bias-correction term $(N_{\rm los} - N_{\rm strips})/(N_{\rm los} - 1)$ combines the bias-correction terms of the individual strips. The remaining distribution of RMs consists of a contribution by the RMs that are built-up outside the Milky Way, and a contribution by the measurement errors in RM. We use a Monte Carlo process to simulate the width of the distribution if there is only noise from the measurement errors, and no astrophysical signal. For each sightline, we draw an RM from a Gaussian distribution with zero mean and a standard deviation that is equal to the measurement error in RM of that sightline. We then determine the standard deviation and variance of the RM distribution of the ensemble of sightlines, and repeat this process 5000 times to build up a distribution of standard deviations and variances. We use the square of the mean standard deviation of these 5000 runs for $\sigma^2_{\rm err}$; using the mean of the variances gives negligible differences for the $\sigma^2_{\rm ERS}$ that we derive.

We estimate the uncertainty in $\sigma_{\rm ERS}$ in equation (A4), ${\rm err}(\sigma_{\rm ERS})$, from the uncertainties in $\sigma^2_{\rm err}$, $\sigma^2_{{\rm MW},i}$,$\langle {\rm RM}\rangle_{{\rm strip}\,i}$, and $\langle {\rm RM}\rangle_{1\,+\,\cdots\,+\,M}$ using the standard expression for error propagation. We did not include the error in $\sigma^2_{\rm RM}$ because this is difficult to estimate; the error in $\sigma_{\rm ERS}$ that we derive should therefore be interpreted as a lower limit on the true error. The error in $\sigma^2_{\rm err}$ depends on whether one uses $\sigma^2_{\rm err} = \langle\sigma_{\rm ERS}\rangle^2$ or $\sigma^2_{\rm err} = \langle\sigma^2_{\rm ERS}\rangle$, but in practice these error terms contribute little to the overall error in $\sigma_{\rm ERS}$ for the ensemble of all sightlines, and for the subsamples of sightlines towards *WISE*–Star and *WISE*–AGN sources. In the first case ${\rm err}(\langle\sigma_{\rm err}\rangle^2) = {\rm SD}(\sigma_{\rm err})/\sqrt{N_{\rm MC}}$, where SD() calculates the standard deviation of the argument and $N_{\rm MC}$ indicates the number of Monte Carlo runs. In the second case ${\rm err}(\langle\sigma^2_{\rm err}\rangle) = {\rm SD}(\sigma^2_{\rm err})/\sqrt{N_{\rm MC}}$.

The other errors are easier to calculate. ${\rm err}(\sigma^2_{{\rm MW},i})$ can be derived from ${\rm err}(\sigma_{{\rm MW},\,i}) \lesssim 0.5\,{\rm rad\,m^{-2}}$ based on how sensitive the model curves in fig. 3 from Schnitzeler (2010) are to even small changes in $\sigma_{\rm MW}$; $\sigma_{\rm MW} = 0.5\,{\rm rad\,m^{-2}}$ is a conservative upper limit. ${\rm err}(\langle {\rm RM}_{{\rm strip}\,i}\rangle)$ and ${\rm err}(\langle {\rm RM}_{1\,+\,\cdots\,+\,M}\rangle)$ can be derived from ${\rm SD}({\rm RM}_{{\rm strip}\ i})/\sqrt{N_i}$ and from ${\rm SD}({\rm RM}_{1+\cdots+M})/\sqrt{N_{\rm los}}$, respectively.

This paper has been typeset from a TEX/LATEX file prepared by the author.